九州大学学術情報リポジトリ
Kyushu University Institutional Repository

Dc Electrical Breakdown of Liquid Nitrogen under Simulated Quench State in Pool Cooled High T_c Superconducting Power Apparatus Pt. 2. Experimental Study of Bubble Behavior and Bubble-Triggered Breakdown Characteristics

Hara, Masanori
Department of Electrical and Electronic Systems Engineering, Kyushu University : Professor

Takano, Koji
Department of Electrical and Electronic Systems Engineering, Kyushu University : Graduate Student

Matsuura, Shunsuke
Department of Electrical and Electronic Systems Engineering, Kyushu University : Graduate Student

Wang, Zhen-Chao
Department of Electrical and Electronic Systems Engineering, Kyushu University : Graduate Student (At present, Eiritu Electronics Industry Co.)

https://doi.org/10.15017/1498315

出版情報：九州大学大学院システム情報科学紀要. 3 (1), pp.35-43, 1997-12-22. 九州大学大学院システム情報科学研究院
バージョン：
権利関係：

KYUSHU UNIVERSITY

九州大学大学院
システム情報科学研究科報告
第3巻　第1号　平成10年3月

Research Reports on Information Science and
Electrical Engineering of Kyushu University
Vol. 3, No. 1, March 1998

Dc Electrical Breakdown of Liquid Nitrogen under Simulated Quench State in Pool Cooled High T_C Superconducting Power Apparatus

Pt. 2. Experimental Study of Bubble Behavior and Bubble-Triggered Breakdown Characteristics

Masanori HARA*, Koji TAKANO**, Shunsuke MATSUURA**
and Zhen-Chao WANG***

(Received December 22, 1997)

Abstract : In the Part 2, observations of thermally induced bubbles and measurements of breakdown characteristics with a cylinder-to-plane gap are described. The experimental results show that observed bubble behavior agrees very well with the analytical one described in the Part 1 and that breakdown voltage in liquid nitrogen in the presence of thermal bubbles depends on activity of boiling and falls down to the value in nitrogen gas at normal boiling temperature. The reduction in breakdown voltage is mainly caused by elongated bubbles in the shortest gap region in smooth cylinder-to-plane gap. Fins on the cylinder reduce the breakdown voltage due to their field enhancement effect, but the reduction by thermal bubbles is minimized if the fin is machined so as to guide electrically the bubble along the groove between fins from a higher external field region to a lower one.

Keywords : Electrical breakdown, Superconducting coil, Fault current limiter, Boiling, Bubble, Vapor locking, Liquid nitrogen

1. Introduction

As stated in Introduction of the Part 1[1], the electrical breakdown phenomena of liquid nitrogen under simulated quench conditions in pool cooled high T_C s.c. power apparatus is studied in this work. Following the theoretical study on bubble behavior in the Part 1, the Part 2 reports experimental results on bubble behavior, breakdown mechanism and breakdown voltage characteristics under simulated quench conditions of s.c. coils and fault current limiters.

Notation of coordinates in the gap and symbols used here are the same as those in the Part 1.

2. Experimental Setup and Procedures

The schematic diagram of the experimental setup for bubble observation and measurement of breakdown voltage characteristics is shown in **Fig. 1**. The cryostat is a double layer glass Dewar vessels usable for experiments with liquid helium. The test liquid in this study is commercial liquid nitrogen at atmospheric pressure. The electrode system consists of a cylindrical electrode with a mounted heater to simulate boiling at quench in s.c. apparatus and a plane electrode. To know the effect of electrode orientation on breakdown phenomena, four arrangements shown in **Fig. 1**(c) in the Part 1 are tested. The gap length and heater power are denoted as g and H which is a ratio of the heater input power to the heater length. The H at boiling onset is indicated by a subscript "$_o$", i.e., H_o.

In practical superconducting wires, fins are often machined on the wire surface for improvement of heat transfer from the wire to surrounding liquid[2]. To simulate non-uniform field by the fins, triangular fins

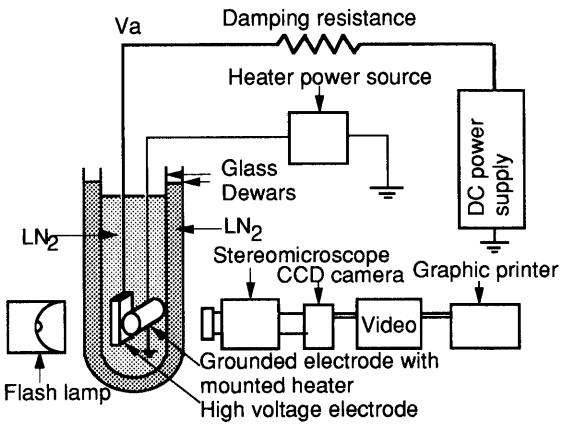

Fig. 1 Schematic diagram of experimental setup.

* Department of Electrical and Electronic Systems Engineering
** Department of Electrical and Electronic Systems Engineering, Graduate Student
*** Department of Electrical and Electronic Systems Engineering, Graduate Student (At present, Eiritu Electronics Industry Co.)

are made on the cylinder surface. Fin shape and dimension are the same as those illustrated in **Figs. 1**(b) and **2**(a) in the Part 1. However, the fin-tip shape of the tested CL electrode is slightly sharper than that of the tested CC one, since the machine for making the CC fin differs from that for the CL fin.

The experiments were conducted as follows. At first, the heater power was set to a desired value, and then the dc applied voltage was raised at a rate of about 1 kV/s until breakdown. The bubble behavior was observed through an opening slit on the glass Dewar wall with back illumination by a stroboscope at a concerned applied voltage. The polarity for characteristics will be indicated as one on the cylindrical electrode later.

At an early stage of this work[3)-4)], the bubble shape was photographed directly by a still camera with a stereoscope, but at a later stage, the boiling under high electric field was observed and recorded by using a CCD camera and video system.

3. Observation of Bubble Behavior

3.1 Suspended Bubbles in Smooth Cylinder-to-Plane Gap

Motion of the suspended bubble is thought to be affected mostly by the gradient force due to the macroscopic field, because the microscopic non-uniform field is limited near the fin, as described in the Part 1. The behavior of suspended bubble was then observed mainly with the CS-II electrode system. The pictures in **Fig. 2** show bubbles generated by the boiling under different applied voltages. **Fig. 2**(d) includes a spark which occurs at the shortest gap region. The values of $\sqrt{H/H_o}$ and g are 2.01 and 2mm, respectively. Since the H_o was 0.15W/mm, the studied value of $\sqrt{H/H_o}$ corresponds to that for the active nucleate boiling. From these pictures, the following are recognized.

1) The electric field causes a decrease in the number of active nuclei and a decrease in bubble diameter.

2) At a higher voltage near breakdown, the electrical gradient force acting on a suspended bubble in the gap becomes predominant for bubble motion as compared with buoyancy. This agrees well with the expectation by the analysis of bubble trajectory[1)].

3) Bubbles around the stagnation line, where the gradient force balances with the buoyancy, form a tight vapor locking at lower applied voltages as seen in **Fig. 2**(b) but change to a chain-like vapor bridge consisting of separated bubbles near the breakdown, as seen in **Fig. 2**(c).

4) The location of the chain-like vapor bridge moves away from the shortest gap region with increasing applied voltage.

In the following, causes of the above observed phenomena will be discussed.

Effect of electric field on bubble generation

According to the study of boiling phenomena without electric field, the bubble at the boiling onset is nearly semi-spherical at early stage of bubble growth, as shown in **Fig. 3**(a), or slightly tear drop in shape when it departs from the electrode surface. With increasing heater power, the bubble shape becomes

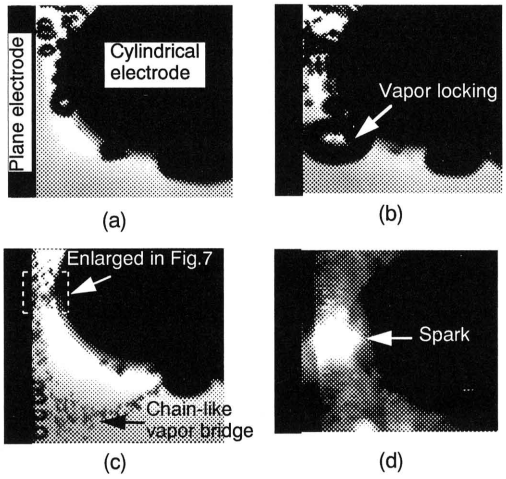

Fig. 2 Boiling phenomenon at different applied voltages with the CS-II electrode system, g=2mm and H=0.61W/mm
(a) V_a=0kV, (b)10kV, (c)30kV, (d)Breakdown.

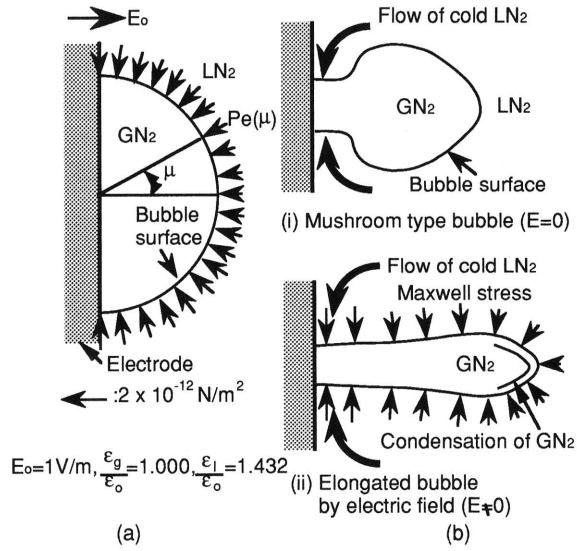

Fig. 3 Surface state of bubbles on electrode
(a) Distribution of Maxwell stress on semispher-eical bubble surface
(b) Bubble shape on electrode at different fields.

like a mushroom, as shown in **Fig. 3**(b-i). When the voltage is applied, the electrical pressure on the surface of semi-spherical bubble depends on the position and is given as

$$P_e(\mu)=\frac{9\varepsilon_l(\varepsilon_l-\varepsilon_g)}{2(2\varepsilon_l+\varepsilon_g)^2}E_0^2(\varepsilon_g\cos^2\mu+\varepsilon_l\sin^2\mu) \quad (1)$$

where ε_g and ε_l are permittivities of gas inside the bubble and surrounding liquid, E_o the external electric field and μ the angle given in **Fig. 3**(a). Since $P_e(\mu=\pi/2)/P_e(\mu=0)=1.43$, the electric field acts as to elongate the bubble in the direction of electric field. This nonuniform electrical pressure is thought to create an elongated bubble on the cylinder surface (**Fig. 3**(b-ii)) and results in a decrease in bubble diameter. The observed ratio of the major to minor semi-axis of suspended bubble under an electric field is much larger than that estimated according to the theory by Garton and Krasucki[5]. This may be due to the mushroom shape at the bubble generation process and additional deformation caused by vibration on the way of bubble motion.

The decrease in the number of active nuclei near the boiling onset may be caused by promotion of cooling by electric field.

Bubble trajectory and bubble coalescence

If the number of active nuclei is reduced near the boiling onset by lowering heater power, a bubble chain released from a given nuclei will align along the bubble trajectory which can be estimated theoretically. Bubble observations were done to confirm this phenomenon with a low heater power.

The observed bubble chain is compared with the calculated bubble trajectories with the CS-II electrode system, g=0.8mm and V_a=11kV. Although the interaction between bubbles was ignored and bubble radius was set as a=0.08mm in the calculation, the estimated trajectory agrees very well including bounce phenomena of bubble on the plane electrode as seen in **Fig. 4**. In this case no overshoot appears in both of the theory and experiment, and the occurrence of bubble coalescence is recognized near the estimated stagnation line.

Voltage dependence of measured bubble-stagnation location y_t (y at $F_{gy}=F_B$) at x=0.4mm agrees fairly well with the estimated one, as shown in **Fig. 5**.

Effect of gap length and heater power on bubble behavior

When the gap length is short so as to be comparable with specific size of thermally induced bubble, the bubble under no applied voltage bridges over the gap,

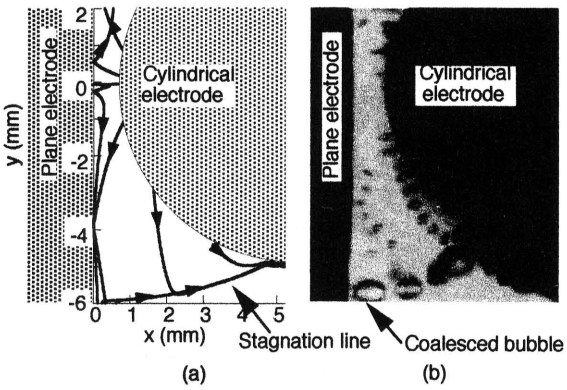

Fig. 4 Comparison of theoretical and experimental bubble trajectories with the CS-II electrode system, g=0.8mm and V_a=11kV
(a) Calculated bubble trajectories.
(b) Photograph of boiling.

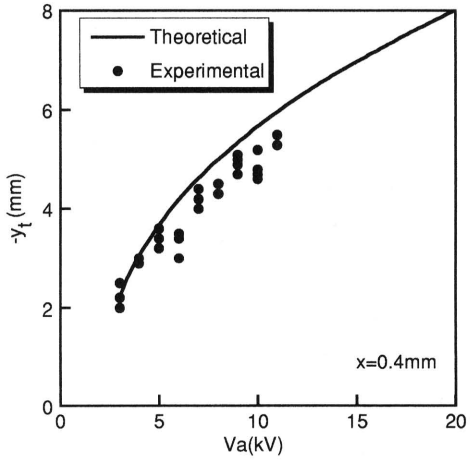

Fig. 5 Voltage dependence of bubble stagnation location with the CS-II electrode system, g=0.8mm and H=1W/mm.

as shown in **Fig. 6**(a). Decreasing gap length shorter than 0.5mm, vapor bridging in the shortest gap region can appear, and the coalesced bubble near the stagnation line touches the cylinder till near the breakdown voltage, as shown in **Fig. 6**(c). In contrast to this, increasing gap length over the specific bubble size, vapor locking occurs only in a limited region of applied voltage, and no bubble bridge appears at any place in the gap near the breakdown voltage. The outline of bubble behavior with the short and long gaps is similar to the previous description for **Fig. 2** except the above statement.

Fig. 7 shows the enlarged sketch of the shortest gap region in **Figs. 2**(c) and **6**(c) which are the photographs near the breakdown voltage. Clearly, the bubble was deformed markedly by a high electric field. With the

short gap, the deformed bubbles bridge over the gap, as seen in **Fig. 7**(b), and their thickness and number increase with the heater power, while the long gap is occupied by discrete deformed bubbles, as seen in **Fig. 7**(a). With increasing heater power, size and number of bubbles increase, while the distance between them decreases. Breakdown occurred through these bubbles in the shortest gap region.

Fig. 8 shows the change in the bubble behavior with applied voltage and heater power with the CS-II electrode system of g=2mm. "Gradient force dominant region" in the figure means that a large part of bubbles leaving from the down side of the cylinder is directed downward and forms the chain-like vapor bridge. "Locking" reveals the vapor locking shown in **Fig. 2**(b) and appears at a relatively high heater power. The broken line in the figure is the theoretically estimated voltage for the onset of stagnation line bridging over the gap. The measured voltage for the formation of vapor locking is slightly higher than the theoretical one.

According to observations with g=20mm, almost all bubbles are rising and no stagnation line is observed till 60kV, the withstand voltage of bushing equipped in the present setup. This agrees with the estimated one described in the Part 1.

Effect of electrode arrangement

Spatial distribution of bubbles and spark at breakdown for the electrode arrangements II, III and IV with the CS cylinder and g=0.8mm are shown in **Fig. 9**(a). In any arrangement, deformed bubbles shown in **Fig. 7**(a) exist in the shortest gap region when the nucleate boiling is active. As expected from the trajectory calculation, the clear stagnation is formed only in the CS-II electrode system. With the CS-III and IV electrode systems, continuous bubble flow from the shortest gap region to the outside occurs but no stagnation appears.

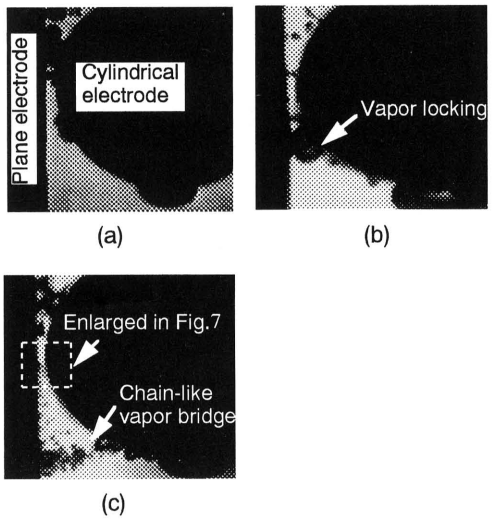

Fig. 6 Boiling phenomena with CS-II electrode system, g =0.5mm and H=0.66W/mm
(a) V_a=0kV, (b) 2kV, (c) 9kV.

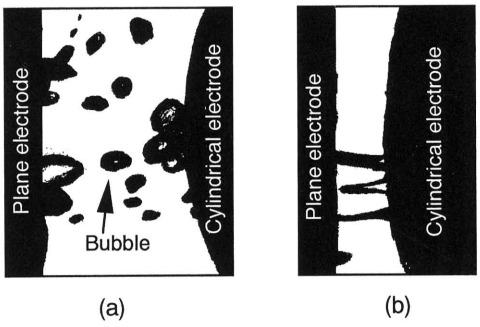

Fig. 7 Enlarged sketch of the shortest gap region in **Figs. 2**(c) and **6**(c).
(a) Enlarged in **Fig. 2**(c),
(b) Enlarged in **Fig. 6**(c).

3.2 Trapped Bubble in Groove

Similar pictures to that with the CS are shown in **Figs. 9**(b) and (c) for the electrode arrangements II, III and IV with the CC and CL cylinders. In these gaps, the stagnation of suspended bubbles occurs only at the arrangement II. Marked difference from the CS electrode in bubble behavior is the occurrence of vapor flow along the groove with the CC and CL.

Shape of trapped bubble was observed with the CC-I

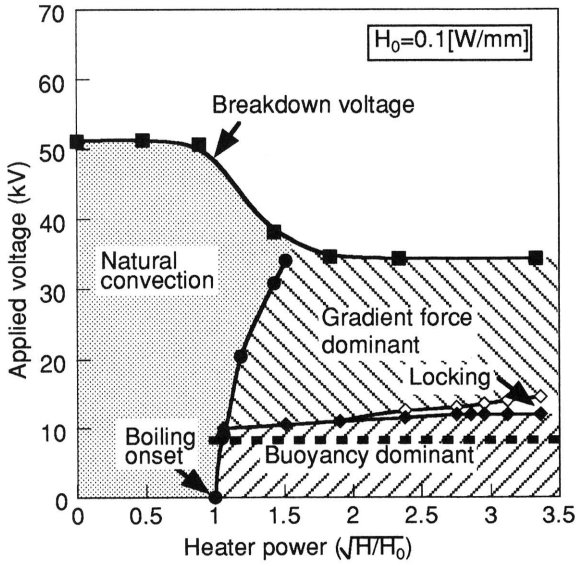

Fig. 8 Region of characterized bubble behavior with CS-II electrode system and g=2mm.

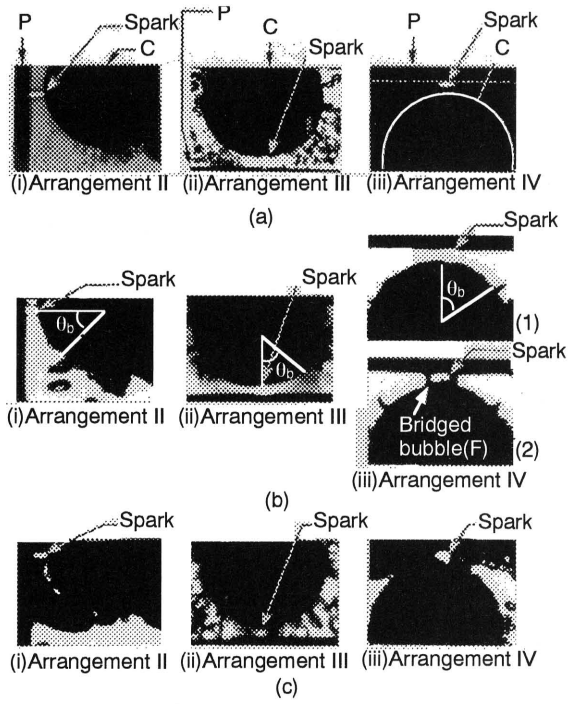

Fig. 9 Bubbles at breakdown voltage with different electrode systems, g=0.8mm and H=0.45W/mm
(a) CS electrode system,
(b) CC electrode system,
(c) CL electrode system.

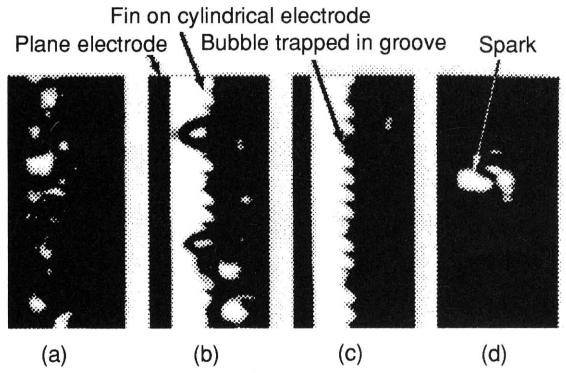

Fig. 10 Bubbles observed from y-direction and with the CC-I electrode system, g=0.8mm and H=1W/mm
(a) V_a=0kV, (b) 13.5kV, (c) 16kV, (d) Breakdown.

electrode as shown in **Fig. 10**. According to rough measurements of shape and size of tightly trapped bubble at the applied voltage of 14-20kV, the principal radii r_1 and r_2 of bubble surface are around 0.2-0.4mm and 5mm (=radius of cylindrical electrode), and the top of bubble surface locates at 0.2-0.3mm from the groove bottom. It is concluded from these measurements that $\boldsymbol{P}_e+\boldsymbol{P}_\sigma=\boldsymbol{P}_v-\boldsymbol{P}_a\fallingdotseq 50\mathrm{N/m^2}$. The $\boldsymbol{P}_e+\boldsymbol{P}_\sigma$ increases with bubble growth since the external electric field increases with the distance from the groove bottom as indicated by the broken line in **Fig. 2** of Part 1. That is, the increment in gas pressure inside the trapped bubble by Maxwell stress and surface tension is believed to be in the order of $100\mathrm{N/m^2}$.

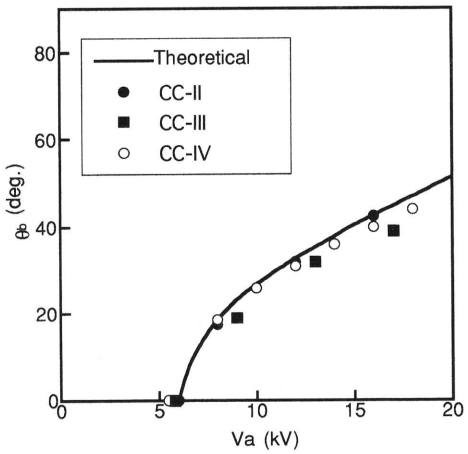

Fig. 11 Comparison of measured and theoretical values of bubble-releasing point from groove with the CC-II, CC-III and CC-IV electrode systems.

With the CC cylinder, fins guide vapor electrically along the groove from a higher external field region to a lower one and bubbles are released from there, i.e., at the θ_b as shown in **Figs. 9** (b-i) and (b-ii). However, vapor in the shortest gap region grows rarely into the gap and then retrogrades again into the groove with the CC-IV electrode as denoted by F in **Fig. 9** (b-iii-(2)). This phenomenon can be described by distribution of hydraulic pressure $\boldsymbol{P}_s$ around the cylinder which was shown in **Fig. 18** in the Part 1. Only with the IV arrangement, the local minimum in the distribution of $\boldsymbol{P}_s+\boldsymbol{P}_e$ occurs near $\theta=0$ and the bubble growth into the gap from there is possible. The θ_b was measured as a function of applied voltage and compared with the calculated one, as shown in **Fig. 11**. In the calculation of θ_b, the release of bubble from the groove was assumed to occur when the Maxwell stress at the point C in **Fig. 3** in the Part 1 decreases below 100 $\mathrm{N/m^2}$. In conclusion, behavior of trapped bubble in the groove can be represented as the conceptual figure shown in **Fig. 19** in the Part 1.

With the CL cylinder, the trapped bubble in the high field region flew normally along the groove to the edge of the cylinder and was released from there. But some bubbles overcame the fin to the lower field region. This is very severe for dielectric withstand, since the sharp fin-tip is covered by the gas and it triggers spark at a lower voltage.

4. Breakdown Mechanism and Breakdown Voltage Characteristics

The breakdown voltage was measured at least five times at each experimental condition and their mean value was plotted in the relevant figures except for the measurement of breakdown probability density function, as will be described later.

4.1 Smooth Cylinder

Breakdown voltage and breakdown mechanism

Typical measured breakdown voltage vs. heater power characteristics with the gaps of 2 and 0.5mm are illustrated in **Fig. 12**. In this figure, the parameter of heater power is given as $\sqrt{H/H_o}$ for enlarged expression of characteristics near the boiling onset heater power. When the heater power increases from zero, the breakdown voltage starts to decrease at the boiling onset and falls down to a critical value, depending on the gap length at about twice the boiling onset heater power. Beyond this heater power, breakdown voltage keeps a nearly constant value. The lowest value is identical with the gaseous breakdown voltage at normal boiling temperature at the short gap of 0.5mm, where the deformed bubble in the shortest gap region could bridge over the gap near the breakdown voltage, as seen in **Fig. 7**(b). However, at the longer gap, where the shortest gap region is occupied by a composite of collective deformed bubbles and surrounding liquid, as shown in **Fig. 7**(a), the breakdown voltage is considerably higher than the gaseous one at normal boiling temperature.

On the way of falling from the start of reduction in the breakdown voltage to the critical value, a high scattering appears in the measured breakdown voltage. In order to gain some insight on the breakdown mechanism and the cause of the high scattering in breakdown voltage, the breakdown probability density distribution was measured with the gaps of g=0.5 and 2mm.

The results are similar in both gaps and are illustrated in **Fig. 13** for g=2mm. At low and high heater powers, the distribution becomes a single-apexed statistical probability density distribution for each. On the other hand, in a heater power region giving a large falling rate of breakdown voltage against the heater power, two distributions may partly overlap. It is concluded from observations of bubble behavior at large reduction in breakdown voltage that the cause of the reduction is the spark-triggering effect of distorted bubble in the shortest gap region and the bridging effect by bubble gas there. The existence of collective distorted bubbles is very unstable and on the way of voltage rise, the bubbles often disappear suddenly from the gap space completely at the large falling rate of the breakdown voltage. The double-apexed distribution in **Fig. 13** may have resulted from this instability. That is, the low-voltage collective in the distribution is by the bubble-triggered breakdown and the high voltage one is by the breakdown at a condition of much lower and less effective concentra-

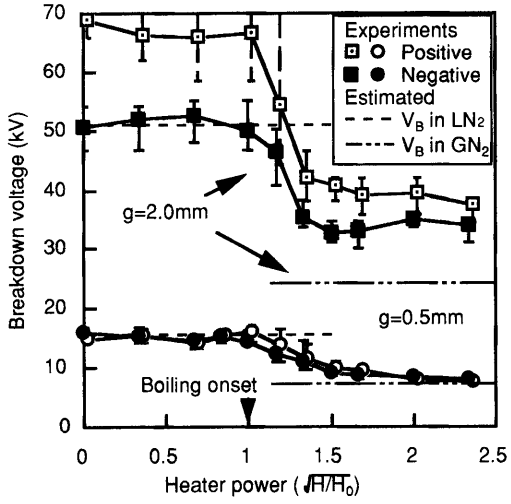

Fig. 12 Characteristics of breakdown voltage vs. heater power with the CS-II electrode system and g=0.5 and 2mm.

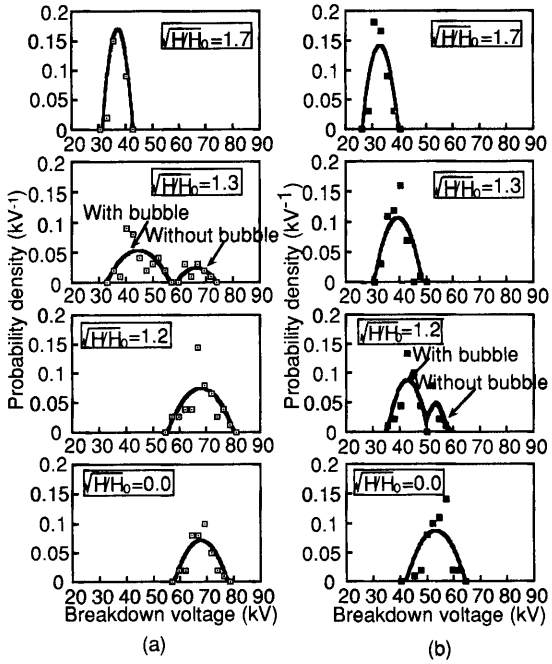

Fig. 13 Breakdown probability density distribution with the CS-II electrode system and g=2mm.
(a) Positive cylinder, (b) Negative cylinder.

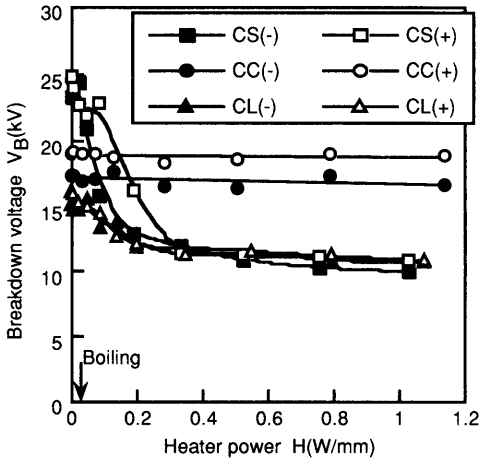

Fig. 14 Polarity effect in breakdown voltage with the II electrode arrangement and g=0.8mm.

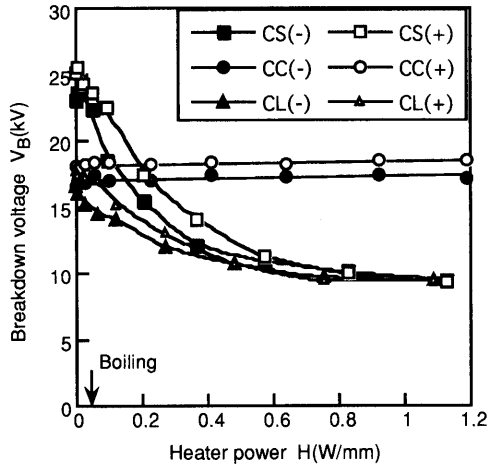

Fig. 15 Polarity effect in breakdown voltage with the I electrode arrangement and g=0.8mm.

tion of thermal bubbles. With higher heater powers, the shortest gap region is filled with more densely distorted bubbles, and breakdown voltage tends to reach the low-collective in the double-apexes.

Polarity effect

The polarity effect is slight at the short gap of 0.5mm, but it becomes remarkable at longer gaps, as seen in **Fig. 12**, since the electric field distribution is approximately uniform in the short gap. In the tested region of gap length, the negative breakdown voltage is lower than the positive one.

4.2 Finned Cylinder

Effect of the fin on breakdown voltage is investigated in detail with different finned cylinders of g=0.8 mm gap. The abscissa in the following breakdown voltage characteristics is denoted by the heater power in contrast with **Fig. 12**.

Polarity effect

To determine the polarity in the following measurement of breakdown voltage characteristics, the polarity effect was investigated previously, as shown in **Figs. 14** and **15**, where the boiling onset heater power was about 0.035W/mm for the tested cylinders. Since the polarity of applied voltage was changed under a given electrode system, effect of irregularity in the fin-tip shape on breakdown voltage could be eliminated in the experiments and then the polarity effect can be observed experimentally from comparison of two curves by the different polarity.

Clearly, the negative breakdown voltage is slightly lower than the positive one for any electrode. Then the negative characteristics are investigated in the following.

Negative breakdown voltage

From **Figs. 14-16**, the following are recognized. For comparison, the characteristics stated previously for the CS electrode are described briefly, too.

1) When the heater power increases for the CS electrode system, breakdown voltage decreases very slowly till the boiling onset, then falls rapidly in the region of 0.035-0.4W/mm, and thereafter keeps a nearly constant value, regardless of the electrode arrangement. This tendency is basically the same as the description for **Fig. 12**. Characteristics of the CL electrode system show the similar tendency with the CS one, but the breakdown voltage is lower and the reduction rate is smaller than those of the CS one in a small heater power region.

2) With the CC electrode system, breakdown voltages for the arrangements of I, II and III are almost independent of the heater power, but it, for the case of IV, shows accidentally two separate values at higher heater powers as shown by symbols ○ and ● in **Fig. 16**(b).

3) Breakdown voltages of the CS electrode at H=0 are in the range of 23-26kV which is approximately equal to the lowest envelope of measured values with quasi-uniform field gaps by many researchers[6], i.e., $V_B=29g^{0.8}$kV where the g is gap length in mm.

The measured breakdown voltage of 9.5-12kV at higher heater power is nearly the same as that in nitrogen gas at normal boiling temperature, i.e. 10kV.

4) Breakdown voltages of CC electrode at H=0 are in the range of 16-18kV which is approximately equal to the lowest envelope of measured values with a point-to-plane gap in liquid nitrogen by many researchers[7], i.e., $V_B=18g^{0.26}$kV.

5) The measured breakdown voltages ranging from

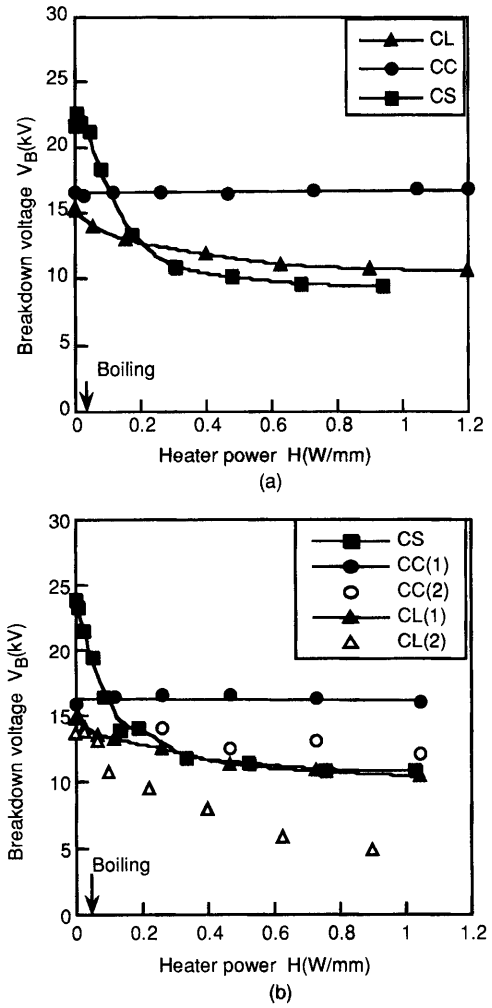

Fig. 16 Effect of heater power on negative breakdown voltage with III and IV electrode arrangements and g=0.8mm.
(a) Arrangement III, (b) Arrangement IV.

15-17kV for the CL electrode at H=0 are slightly lower than that of CC electrode due to sharper fin tip on the CL described previously. While it shows two separate values at higher powers, as shown by symbols △ and ▲ in **Fig. 16**(b), the upper one is 9-12kV and the lower one is 7kV as compared with 8kV for normal saturation gas.

Breakdown mechanism

Effect of fin on breakdown mechanism is described on the basis of bubble observation and breakdown characteristics as follows:

1) With the CC electrode, no bubble appears near the fin tip and no suspended bubble is in the shortest gap region for any electrode arrangement, except for rare cases as shown in **Fig. 9**(b-iii-(2)), where the trapped bubble grows unstably into the gap. In this case, breakdown occurs in liquid nitrogen in the absence of thermal bubble, and its voltage is independent of the heater power as shown by the symbol ● in **Fig. 16**(b). When the trapped bubble grows out of the groove near θ=0 as shown in **Fig. 9**(b-iii-(2)), however, breakdown voltage decreases close to the gaseous value at higher heater power as shown by the symbol ○ in **Fig. 16**(b). It should be noted that the latter values are always higher than those for the CS electrode. This is believed to be so due to the existence of a thin liquid layer on the plane electrode which is inferred from the rounded bubble shape there.

2) In the case of CL electrode, bubble coming over the fin tip from a higher external field region to a lower one was always observed during experiments by using a certain cylinder, but with other cylinders it never appeared. This overflow is considered to be due to an obstruction to bubble flow along the groove, such as foreign particle clinging to the groove bottom. When the fin is covered by the overflow bubble, breakdown voltage falls severely and becomes the lowest among the measured ones as shown by the symbols △ in **Fig. 16**(b).

4.3 A Prevention Measure for Reduction of Breakdown Voltage by Thermal Bubbles

From a view point of manufacturing of superconducting wires, the longitudinal finning is easier than the circular finning. However it is concluded from the above descriptions that machining fins, so as to guide electrically a bubble along the groove from a higher field region to a lower one, is important to maintain a high dielectric strength under active boiling conditions. This desired bubble flow can be obtained by forming a groove along the direction of gradient force on the electrode or making fin in island-shape like a pin.

5. Conclusion

Observations of bubble behavior and measurements of breakdown voltage with cylinder-to-plane gaps in liquid nitrogen were performed with dc applied voltage, and breakdown mechanism in the presence of thermal bubble was discussed. The cylinder surface was smooth or grooved circularly or longitudinally. The results may be summarized as follows.

1) Observed bubble behavior, such as bubble trajectory, bubble coalescence near the stagnation line, blowing-off effect of fin on bubbles near the fin-tip, and bubble trap in the groove, agrees very well with the theoretical expectation described in the Part 1.

2) Negative breakdown voltage is lower than the positive one in the tested gaps, g=0.5-2mm.

3) Negative breakdown voltage with a smooth or longitudinally finned cylindrical electrode decreases with the boiling activity. The lowest value reaches down to the gaseous breakdown voltage at normal boiling temperature.

4) Negative breakdown voltage with a circularly finned cylindrical electrode is independent of the boiling.

5) Reduction in breakdown voltage by boiling is mainly caused by the existence of bubble in the shortest gap region, i.e. spark-triggering effect and gas-bridging effect by distorted bubbles.

6) Bubble coalescence and formation of vapor locking along the stagnation line do not cause the reduction in the breakdown voltage since its location is away from the shortest gap region.

7) Double-apexed distribution in the breakdown probability density distribution was observed in a heater power, giving a large reduction rate of breakdown voltage against the heater power. This comes from unstable existence of bubble in the shortest gap region.

8) The reduction in breakdown voltage by thermally induced bubble can be minimized by machining fin so as to guide electrically the bubble along the groove between fins from a higher external field region to a lower one.

Acknowledgements

This work was supported in part by a Grand-in-Aid for Scientific Research from Ministry of Education, Science and Culture, Japan.

References

1) M. Hara, Z. C. Wang, S. Matsuura and K. Takano: Research Reports on Information Science and Electrical Engineering of Kyushu University, Vol. 3, No. 1, pp. 23-33 (1998)
2) S. Shimamoto, T. Ando, T. Hiyama, H. Tsuji, K. Yashida, E. Tada, M. Nishi, K. Okuno, K. Koizumi, K. Oka and K. Yasukouchi: Proc. of 8th Symposium on Engineering Problem of Fusion Research", San Francisco, pp. 1174-1178 (1978)
3) M. Hara, Z. C. Wang and H. Saito: Proc. 8th ISH, Yokohama, Japan, Paper No. 93.01 (1993)
4) M. Hara, Z. C. Wang and H. Saito: IEEE Trans. on DEI, Vol. 1, pp. 709-715 (1994)
5) C.G. Garton and Z. Krauscki: Proc. Roy. Soc. A280, pp. 211-226 (1964)
6) M. Hara, H. Koishihara and K. Saita: IEEE Trans. on EI, Vol. 26, pp. 685-691 (1991)
7) M. Hara: Cryogenic Engineering (of Japan), Vol. 24, pp. 22-81 (1989)